Enhanced Absorption of a Patterned Thin Germanium Layer as a High-Contrast Grating

Yijin Zhang, Xiyuan Cao, Yanyue Ding, Zhongying Xue, Xiaoyu Liu, Shifeng Li, Jian Sun, Yi Jin, and Aimin Wu

***Abstract*—Absorbers such as photonic crystals, metasurfaces, and nanowires have been demonstrated to have important applications in solar cells, detectors, etc. The application of thin-layer-based absorbers to photodetectors is beneficial to simultaneously improve responsivity and 3 dB bandwidth. In this work, we propose a high-contrast-gratings-like absorber to achieve ultra-high absorption based on a thin Germanium layer. High absorption approximately 95% at wavelength 1310 nm is reached for TE-polarized incidence due to the interference of two guided modes, which is 4 times compared to the planar film with the same thickness. The high absorption of the absorber is also experimentally demonstrated. This work shows a new method for enhanced absorption with thin Germanium layer, indicating a promising prospect for high-efficiency photodetection.**

***Index Terms*—Enhanced absorption, high-contrast-gratings-like, guided mode, germanium.**

I. Introduction

OPTICAL interconnection based on silicon photonics is considered as an ideal solution to meet the demands of ultra-fast connection and switch in the big data information era due to its capability of large-scale integration, which can offer ultra-broadband optical transmission [1], [2]. As a key component of optical transceiver that convert optical signals into electrical signals, photodetectors (PDs) have received widespread attention. Germanium (Ge) is widely used in near-infrared (NIR) photodetection for its energy bandgap of 0.66 eV [3], [4], [5], and it's also a Complementary Metal Oxide Semiconductor (CMOS) compatible material. For photodetection, it is important to use a thinner active layer for shorter carrier transit time to achieve larger 3dB bandwidth. However, thinner active layer is accompanied by lower responsivity due to the weak inherent absorption coefficient efficiency of Ge [6], [7], [8]. Breaking the inherent bandwidth-efficiency trade-off, i.e., improve the absorption efficiency of thin active layer, has attracted intensive research, which is also an important solution to reduce power consuming of the entire system.

A lot of work has been done for increasing absorption of the thin active layer. The cavity-enhanced absorption is mostly used in earlier work [9], [10], the light is reflected multiple times between the top mirror and bottom mirror to increase the interaction of the light and the material, but the design of the multilayer resonant cavity will bring complexity to the fabrication processes. The plasmonic effect of metals is another suggestion to optimize the absorption [11], [12], while metal will bring additional heat energy and is not compatible with CMOS technology. There are also studies based on heterojunction PDs by introducing materials such as monolayer graphene [13], [14], perovskite [15] into the device, the Schottky junctions formed by heterogeneous material layer and Ge thin layer contact will speed up the separation of photogenerated carriers, however, this method is limited in improving the responsivity and does not fundamentally solve the bandwidth-efficiency contradiction. In recent years, the development of nanophotonics has provided new ideas for improving the absorption of thin active layer, photonic crystals, metasurfaces, nano-antennas, nanowires and etc. are simple in design and easy to integrate with surface-illuminated PDs, thus attracting more and more attentions [16], [17]. For example, periodic photon-trapping micro- and nanoholes integrated in Si photodiodes can generate lateral propagating slow and stationary optical modes upon light incidence [17], this Si photodiode exhibits more than 52% external quantum efficiency (EQE) at 850 nm, which is 8 times higher than that of a Si photodiode with a flat surface designed with an active layer thickness of 1.3 μm. It's important to design all-dielectric germanium nanostructure to obtain high absorption in the communication band for high efficiency photodetection.

Manuscript received 25 July 2022; revised 6 September 2022; accepted 8 September 2022. Date of publication 20 September 2022; date of current version 30 September 2022. This work was supported in part by the National Key Research and Development Program of China under Grant 2021YFB2206502, in part by the National Natural Science Foundation of China under Grant 61875174, in part by the Youth Innovation Promotion Association of the Chinese Academy of Sciences under Grant 2021232, and in part by the Shanghai Sailing Program under Grant 19YF1456600. *(Corresponding authors: Yi Jin; Aimin Wu.)*

Yijin Zhang, Yanyue Ding, Zhongying Xue, Xiaoyu Liu, and Aimin Wu are with the State Key Laboratory of Functional Materials for Informatics, Shanghai Institute of Microsystem and Information Technology, Chinese Academy of Sciences, Shanghai 200050, China, and also with the Center of Materials Science and Optoelectronics Engineering, University of Chinese Academy of Sciences, Beijing 100049, China (e-mail: yjzhang@mail.sim.ac.cn; yanyue.ding@mail.sim.ac.cn; simsnow@mail.sim.ac.cn; xiaoyuliu@mail.sim.ac.cn; wuaimin@mail.sim.ac.cn).

Xiyuan Cao is with the State Key Laboratory of Dynamic Measurement Technology, North University of China, Taiyuan 030000, China (e-mail: caoxiyuan@nuc.edu.cn).

Shifeng Li is with the College of Engineering and Applied Science, Nanjing University, Nanjing 210023, China (e-mail: lishifeng@nju.edu.cn).

Jian Sun is with the Engineering Research Center of Ultra-Precision Optical Manufacturing (Shanghai), Department of Optical Science and Engineering, School of Information Science and Technology, Fudan University, Shanghai 200433, China (e-mail: jsun@fudan.edu.cn).

Yi Jin is with the Centre for Optical and Electromagnetic Research and International Research Center for Advanced Photonics, College of Optical Science and Engineering, Zhejiang University, Hangzhou 310058, China (e-mail: jinyi_2008@zju.edu.cn).

Digital Object Identifier 10.1109/JPHOT.2022.3207805

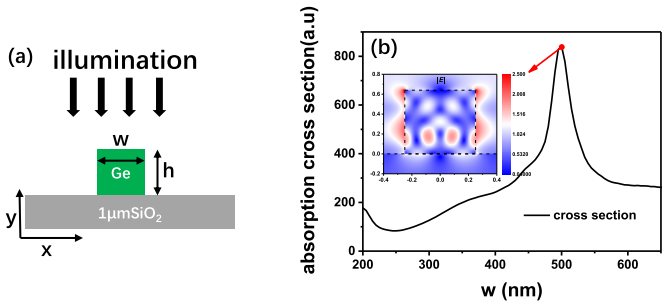

Fig. 1. Single Ge strip. (a) Schematic of the single Ge strip ($h = 640$ nm). (b) Absorption cross section with changing w at wavelength 1310 nm normal TE incidence, inset shows the normalized electric amplitude distribution $|E|$.

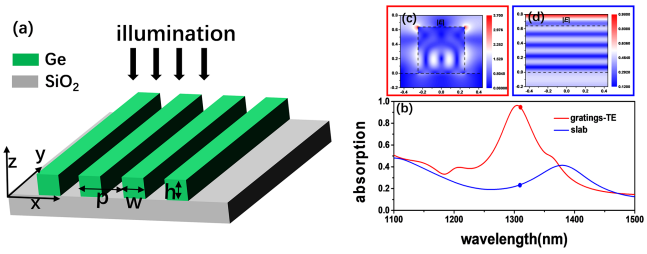

Fig. 2. HCG-like absorber. (a) Structure configuration. ($p = 880$ nm, $w = 500$ nm, $h = 640$ nm). (b) The simulated absorption of the presented absorber under TE-polarized NI (red, solid line) and the referential slab without nanostructure (blue, solid line). The normalized electric amplitude distributions at wavelength 1310 nm of the absorber under TE-polarized NI (c) and the unstructured referential slab (d) are respectively given.

High-contrast grating (HCG) has significant advantages in efficient light modulation due to the high refractive index contrast of the materials, it has been widely used in optical devices such as vertical cavity surface emitting laser (VCSEL) [18], [19], planar focusing reflectors [20], etc. by realizing almost complete reflection or transmission [21], [22]. It has been demonstrated that guided-mode resonance (GMR) can be generated by quasi-guided, or leaky waveguide modes induced on nanostructure with the subwavelength periods [23], [24]. In this work, a Ge HCG-like absorber is proposed to enhance the absorption at NIR wavelengths, ultra-high absorption is achieved near 1310 nm by interference of two guided modes. To demonstrate the high absorption effect, the absorber is fabricated on Germanium-on-Insulator (GOI) substrate, experiments and numerical simulations consistently illustrate the absorption enhancement. This work provides a new method for efficient photodetection in the communication band.

II. Design and Simulations

In order to obtain an ultra-high absorption, we start from calculating the absorption cross section of a single Ge strip as shown in Fig. 1(a), the 640 nm-thickness Ge grating is placed on a 1 μm silica (SiO_2) layer and the whole is placed in a vacuum. Coupling of incident light with leaky mode resonance supported by nanowires can enhance absorption [25], and the light can be trapped in the dielectric material due to multiple total internal reflections caused by high refractive index contrast [26]. For a single Ge strip, the incident light will be more easily localized because of the high refractive index contrast between Ge, air and SiO_2. The size of the absorption cross section can intuitively characterize the probability of the incident light being absorbed by the medium, the absorption cross section is calculated by $\sigma_{abs} = P_{abs}/I_{source}$, which P_{abs} is total power absorbed, I_{source} is the intensity of the light source. The absorption cross section of a single Ge strip is simulated to choose the width (w) of Ge strip which can ensure the maximum absorption for the incident light at wavelength 1310 nm.

The finite-difference time-domain (FDTD) method is used to simulate light propagation in the structure, the optical constants of Ge and SiO_2 are from Palik's handbook [27], and the environment is set as vacuum. Structure is illuminated by TE-polarized (the electric field along the x axis) Total Field Scattering Field (TFSF) source, the simulation region is surrounded by Perfectly Matched Layer (PML) boundaries. Fig. 1(b) shows the dependence between the absorption cross section and width w at wavelength 1310 nm normal TE incidence, one can see that the maximum absorption cross section is reached when the width is 500 nm. The normalized electric amplitude distribution is visualized in the x-y plane as shown in the inset of Fig. 1(b), confirms that the absorbed power is trapped in the Ge strip.

The schematic of the HCG-like absorber is shown in Fig. 2(a) with $w = 500$ nm, $h = 640$ nm and $p = 880$ nm. Fig. 2(b) shows the simulated absorption of the presented absorber at TE-polarized (the electric field along the x axis) normal incidence (NI), the absorption of referential unstructured planar structure with the same thickness is also given. The absorption of the HCG-like absorber we proposed increases significantly in entire O band compared to the unstructured Ge slab. Particularly, approximately 95% absorption can be achieved around wavelength 1310 nm at TE-polarized NI, is about 4 times compared to the unstructured Ge slab. Fig. 2(c), (d) show the normalized electric amplitude distributions on the x-z plane of different situations at wavelength 1310 nm, indicating more confined field localization of the absorber at TE-polarized NI.

Next, Fig. 3(a)–(c) show the numerical simulation of the influence of geometrical parameters on the absorption under TE-polarized NI. It can be clearly observed that this absorber has a tunable resonant wavelength, the absorption is red-shifted with the increase of p, w and h as shown in Fig. 3(a)–(c) respectively. In particular, the resonant wavelength is more dependent on w and h than on p, where the resonant peak position is almost linearly related to w, suggesting that the absorber doesn't depend on the periodic resonance. Synchronously, as shown in Fig. 3(a), when the period broadens from 700 nm to 950 nm, the corresponding absorption peak increases first and then decreases as the period increases. This similar phenomenon can also be observed as w and h increase, which represents that the light absorption state of the absorber is from uncoupled to critically coupled, and then to over-coupled [28].

Supplementally, the additional simulations to investigate the angle dependence are performed in Fig. 4(a), (b). As illustrated by the inset of Fig. 4(a), the incident electric filed is fixed along

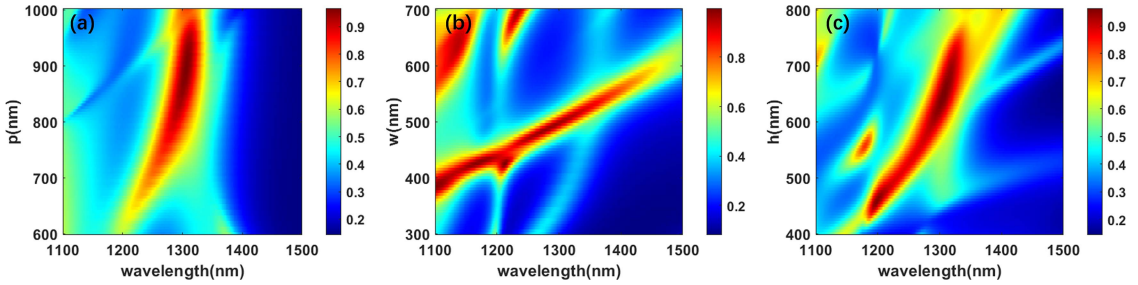

Fig. 3. The influence of varying period p (a), width w (b) and thickness of Ge layer h (c) on absorption under the TE-polarized NIR NI.

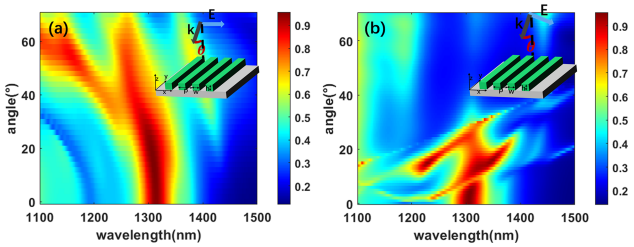

Fig. 4. Influence of incident angle. (a) and (b) Influence of incident angle θ on the absorption. In (a), the incident electric field is polarized along the x direction and the inset illustrates the variation of θ. And in (b), the incident magnetic field is polarized along the y direction and the inset illustrates the variation of θ.

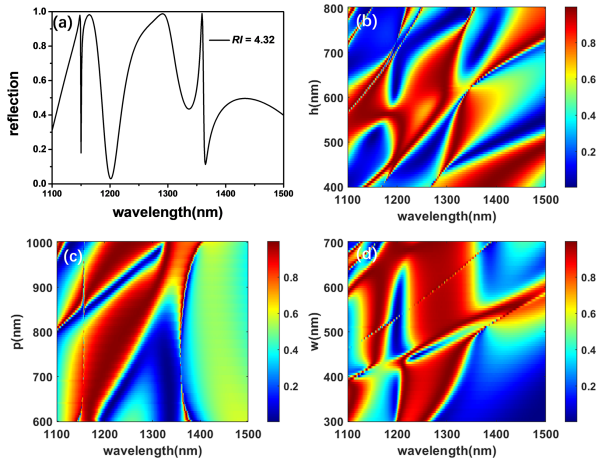

Fig. 5. Reflection properties of HCG-like absorber with lossless Ge. (a) Reflection of HCG-like gratings under TE-polarized NI when Ge is lossless, $p = 880$ nm, $w = 500$ nm, $h = 640$ nm. The influence of varying h (b), p (c) and w (d) on reflection of HCG-like gratings under the TE-polarized NIR NI.

the x direction and the incident angle of θ is varied along the y-z plane, absorption is insensitive when the angle of incident angle is within 30°. In contrast, absorption is very sensitive as shown in Fig. 4(b), the absorption peak disappears rapidly as the angle increases, where the incident magnetic field is fixed along the y direction and the incident angle of θ is varied along the x-z plane. This is due to the first-order diffraction inside the SiO_2 spacer induced by the x-direction period.

In order to further understand the physical mechanism of this HCG-like absorber, the reflection (R) of the gratings under TE-polarized NI with Ge lossless (refractive index RI = 4.32) is studied, in this case, the transmission (T) can be obtained from $T = 1 - R$. Fig. 5(a) shows the reflection of gratings under TE-polarized NIR when $p = 880$ nm, $w = 500$ nm and $h = 640$ nm. Fig. 5(b)–(d) are reflections as a function of h, p and w, respectively. It can be seen that the grating has nearly 100% reflection near 1300 nm, in addition, it has sharp total reflection peak near wavelengths 1148 nm, 1165 nm and 1360 nm, high reflectivity is one of the features of HCG [29], [30]. It can be clearly seen in Fig. 5(b), the total reflection and total transmission (non-reflection) peaks meet around the optimized $h = 640$ nm with increasing h and split into total reflection and total transmission peaks with further increases in h, this indicates that two guided modes interfere with each other around 1310 nm which results in ultra-high absorption. Supplementally, the grating with Ge lossless performs almost total reflection as shown in Fig. 5(a). This property suggests the application prospects of the absorber in saturable absorbers, such as total reflection femtosecond laser [31], [32]. The incident light will be almost totally reflected when the incident light is strong enough to saturate the material absorption.

The above one-dimensional absorber is sensitive to the incident polarization. To fulfill the practical requirement of polarization-insensitive absorption, a symmetrical cross-strip absorber is additionally proposed as shown in Fig. 6(a). The same HCG-like structure is added vertically on the HCG-like absorber, the optimized geometrical parameters are $P = 940$ nm, $W = 330$ nm, $h = 640$ nm, the simulated reflection, transmission and absorption of the cross-strip absorber are shown in Fig. 6(b). Approximately 96.7% absorption can be achieved at wavelength 1310 nm, is about 4 times compared to the unstructured Ge slab. As a profitable by-product of the two-dimensional structure, one can see that the absorption is obviously enhanced within the wavelength range from 1100 nm to 1390 nm. Additionally, the ideal responsivity of PDs with this cross-strip absorber is simulated in Fig. 6(c), assuming 100% internal quantum efficiency. It can be observed that the responsivity is greater than 0.8 A/W in the range of 1290 nm –1370 nm, which is expected to meet the application requirements. Subsequently, the influence of the polarization angle on the absorption is also investigated and shown in Fig. 6(d) (the polarization angle is the angle between the electric field direction and the x-axis). One can clearly see that the absorber is insensitive to the incident polarization.

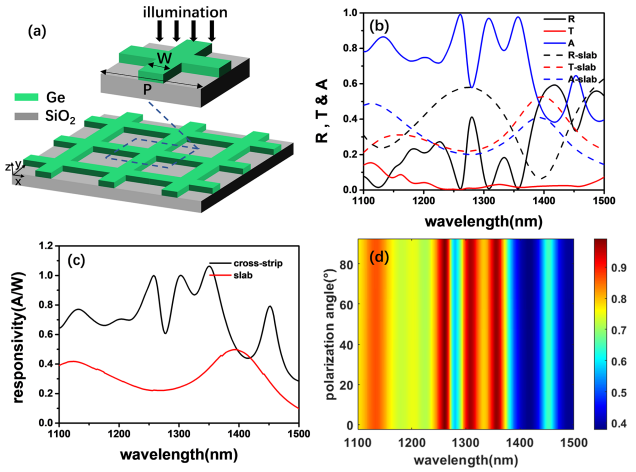

Fig. 6. Cross-strip absorber. (a) Structure configuration. ($P = 940$ nm, $W = 330$ nm, $h = 640$ nm). (b) The simulated reflection, transmission and absorption of the cross-strip absorber and the referential slab without nanostructure. (c) Simulated responsivity of cross-strip absorber and slab in NIR under ideal conditions. (d) Influence of the incident polarization on the absorption.

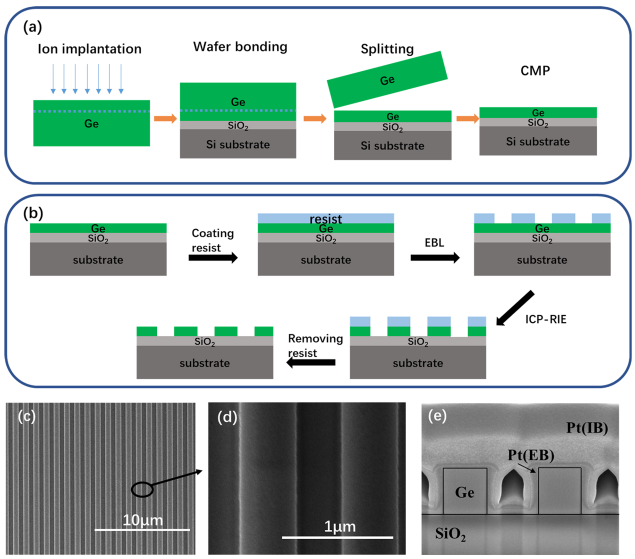

Fig. 7. Preparation of HCG-like absorber. (a) The process flow of GOI preparation using ion-slicing technology. (b) Schematic diagram of the fabrication procedures for Ge HCG-like absorber. The top-view (c), (d) and cross-sectional (e) cross-sectional SEM image of the sample.

III. Experiment

The GOI wafer is prepared by ion-cut technology [33], [34], as shown in Fig. 7(a). The Ge thin film is transferred onto silicon oxide wafer, and it maintains perfect single crystal properties because the transferred Ge film is from a single crystal Ge wafer [35]. The thickness of the top Ge layer and the buried oxide layer are about 670 nm and 1.04 μm, respectively. Next, The Ge HCG-like absorber is fabricated according to the schematic diagram of the process flow shown in Fig. 7(b). The Electron-beam lithography resist (ZEP520A) is spin-coated on the wafer, and then patterned with electron beam lithography (EBL). Inductively coupled plasma reactive ion etching (ICP-RIE, Oxford Plasmalab System 100) is utilized to transfer the pattern to the Ge layer. We characterize the fabricated gratings using scanning electron microscopy (SEM), the top-view and cross-sectional SEM images are shown in Fig. 7(c)–(e). As seen in the cross-sectional view in Fig. 7(e) where the Pt(EB) and Pt(IB) layers are deposited by electron beam and ion beam, respectively, on the Ge grating to increase the surface conductivity for clear SEM imaging, an almost completely vertical cross-sectional shape is obtained that is consistent with the simulation model. For further comparison, series of w from 460 nm to 500 nm with 10 nm increments are obtained (the period $p = 880$ nm).

The fabricated samples are then measured using a micro-spectroscopy system. The absorptance A (λ) is calculated by A (λ) $= 1 - T$ (λ) $- R$ (λ). A glass slide is used as the reference for transmission and a silver mirror is used as the reference for reflection. It should be noted that the difference in RI between the Ge layer in the experiment and the ideal Ge material cannot be ignored, the change in the refractive index may affect the position of the resonant peaks. The RI of a material can be expressed by $n + \mathrm{i} * k$, where n and k represent the real and imaginary parts of the refractive index, respectively. Since SiO_2 and Si are transparent in NIR, the absorption of GOI (670 nm Ge/1.04 μm SiO_2/Si substrate) is mainly attributed to the absorption of the Ge layer, which can be seen as a Fabry-Perot (FP) cavity. The wavelength position corresponding to the absorption peak is mainly determined by n, and the absorption value is determined by k. Therefore, the optical constant of Ge material can be fitted according to the measured absorption of the referential GOI slab. Eventually, the fitted refractive index of Ge material RI(Ge) is $4.1 + \mathrm{i} * 0.1$, the simulation results here are based on the actual geometrical and material parameters.

Fig. 8(a) shows the measured absorption (orange), reflection (olive) and transmission (navy) of the Ge HCG-like absorber with different widths under TE-polarized NIR NI. It can be seen that the absorption is greatly enhanced between 1100 nm and 1300 nm. The absorption peak is nearly 90% around 1250 nm when w is 500 nm, about 4 times compared to the referential unstructured planar structure with the same thickness. The shift of the experimental absorption peak from the numerical result in Fig. 2 is attributed to the difference between the actual optical constant of the fabricated Ge material and that from the data base of the simulation software. To confirm the experimental measurement, we have measured the practical Ge parameter for numerical simulation, and the simulated result is shown in Fig. 8(b). One can see that the numerical simulation is consistent well with the experimental measurement. The remained difference between the measured and simulated results may be attributed to the fabrication imperfection (containing roughness of surface, deformation of shape, etc) and the measurement error. In addition, it can be observed from both simulated and measured absorption spectrum that the absorption is red-shifted as the w increases with a fixed period, that means the absorber is a strong width-dependent absorption. This is due to the strong resonant modes supported in the different width of the strip would efficiently couple the incident light at different wavelengths [36]. The wavelength selectivity of this absorber is beneficial to our design of different target wavelengths, which

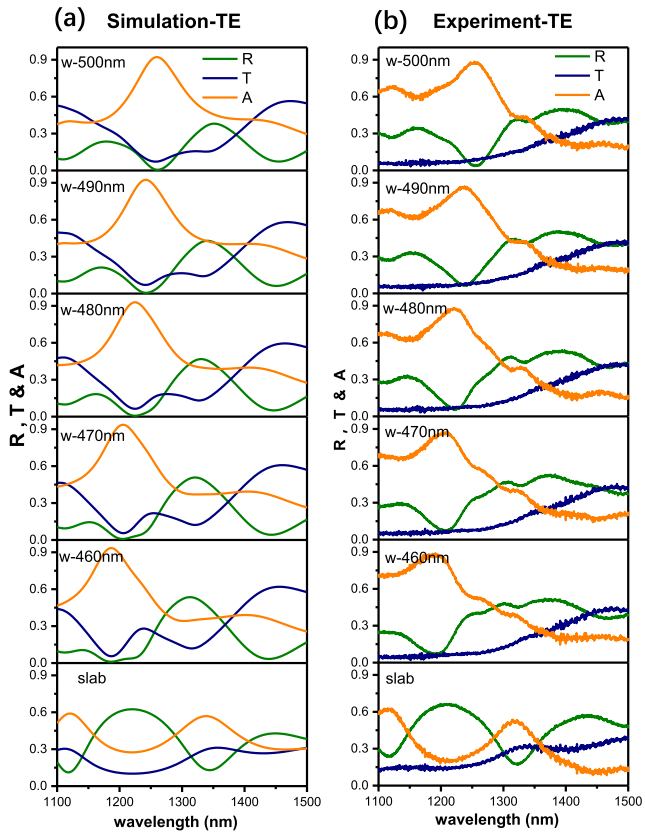

Fig. 8. Experimental results of HCG-like absorber. (a) The simulated absorption (orange), reflection (olive) and transmission (navy) of Ge HCG-like absorber with different widths under TE-polarized NIR NI. The actual thickness of the Ge layer (h) is 670 nm and the fitted refractive index of Ge material RI(Ge) is 4.1 + i ∗ 0.1. (b) The measured absorption, reflection and transmission of gratings with different widths under TE-polarized NIR NI.

is crucial for practical applications. Our proposed absorbers are expected to be integrated into a surface-illuminated vertical-PIN detector [37], [38], the ultra-high absorption is beneficial to improve the responsivity of the PDs. In addition, the thickness of intrinsic Ge layer is expected to be controlled at 500 nm, and the carrier transit-time-limited bandwidth f_T greater than 50 GHz can theoretically be obtained according to $f_T = 0.45 * v_{sat}/d$, where v_{sat} is saturated drift velocity of Ge ($6*10^6$ cm/s) and d is the thickness of intrinsic Ge layer [37], [39], which promise a fast response.

IV. Summary

In conclusion, the Ge HCG-like absorber that effectively enhance absorption in the NIR band is demonstrated theoretically and experimentally. Absorber achieves ultra-high absorption greater than 95% around 1310 nm due to the interference of two guided modes, simultaneously, it has saturable absorption properties. Experimentally, approximately 90% absorption can be achieved around 1250 nm for TE-polarized incidence when the width of the strip is 500 nm, which is increased by 4 times compared to the referential unstructured planar structure with the same thickness. Furthermore, this absorber has an obvious wavelength selectivity and polarization sensitivity, this is beneficial for future applications in detectors. The design of this absorber is simple and the process is compatible with CMOS, that lays the groundwork for future applications in the surface-illuminated PDs.

References

[1] C. Sun et al., "Single-chip microprocessor that communicates directly using light," *Nature*, vol. 528, no. 7583, pp. 534–538, 2015.
[2] S. Assefa et al., "CMOS-integrated high-speed MSM germanium waveguide photodetector," *Opt. Exp.*, vol. 18, no. 5, pp. 4986–4999, 2010.
[3] U. K. Mishra and J. Singh, *Semiconductor Device Physics and Design*. Dordrecht, The Netherlands: Springer, 2008.
[4] U. Otuonye, H. W. Kim, and W. D. Lu, "Ge nanowire photodetector with high photoconductive gain epitaxially integrated on Si substrate," *Appl. Phys. Lett.*, vol. 110, no. 17, 2017, Art. no. 173104.
[5] S. M. Sze, Y. Li, and K. K. Ng, *Physics of Semiconductor Devices[M]*. Hoboken, NY, USA: Wiley, 2021.
[6] Y. Lee et al., "Design study of the gate-all-around silicon nanosheet MOSFETs," *Semicond. Sci. Technol.*, vol. 35, no. 3, 2020, Art. no. 03LT01.
[7] H. Cansizoglu et al., "Surface-illuminated photon-trapping high-speed Ge-on-Si photodiodes with improved efficiency up to 1700 nm," *Photon. Res.*, vol. 6, no. 7, pp. 734–742, 2018.
[8] Y. Lin et al., "High-efficiency normal-incidence vertical p-i-n photodetectors on a germanium-on-insulator platform," *Photon. Res.*, vol. 5, no. 6, pp. 702–709, 2017.
[9] J. Yu, E. Kasper, and M. Oehme, "1.55-μm resonant cavity enhanced photodiode based on MBE grown Ge quantum dots," *Thin Solid Films*, vol. 508, no. 1, pp. 396–398, 2006.
[10] M. K. Emsley, O. Dosunmu, and M. S. Unlu, "High-speed resonant-cavity-enhanced silicon photodetectors on reflecting silicon-on-insulator substrates," *IEEE Photon. Technol. Lett.*, vol. 14, no. 4, pp. 519–521, Apr. 2002.
[11] N. Das, A. Karar, M. Vasiliev, C. L. Tan, K. Alameh, and Y. T. Lee, "Analysis of nano-grating-assisted light absorption enhancement in metal–semiconductor–metal photodetectors patterned using focused ion-beam lithography," *Opt. Commun.*, vol. 284, no. 6, pp. 1694–1700, 2011.
[12] W. Wu, A. Bonakdar, and H. Mohseni, "Plasmonic enhanced quantum well infrared photodetector with high detectivity," *Appl. Phys. Lett.*, vol. 96, no. 16, 2010, Art. no. 161107.
[13] F. Yang et al., "Ultrathin broadband germanium–graphene hybrid photodetector with high performance," *ACS Appl. Mater. Interfaces*, vol. 9, no. 15, pp. 13422–13429, 2017.
[14] S. Q. Li et al., "Vertical Ge–Si nanowires with suspended graphene top contacts as dynamically tunable multispectral photodetectors," *ACS Photon.*, vol. 6, no. 3, pp. 735–742, 2019.
[15] W. Hu et al., "Germanium/perovskite heterostructure for high-performance and broadband photodetector from visible to infrared telecommunication band," *Light: Sci. Appl.*, vol. 8, no. 1, 2019, Art. no. 106.
[16] S. Chugh, S. Goyal, and S. Gupta, "Demonstration of high-speed digital-to-analog conversion using photonic integration," in *Proc. Conf. Lasers Electro-Optics*, 2020, pp. 1–2.
[17] Y. Gao et al., "Photon-trapping microstructures enable high-speed high-efficiency silicon photodiodes," *Nature Photon.*, vol. 11, no. 5, pp. 301–308, 2017.
[18] C. Chase, Y. Rao, W. Hofmann, and C. J. Chang-Hasnain, "1550 nm high contrast grating VCSEL," *Opt. Exp.*, vol. 18, no. 15, pp. 15461–15466, 2010.
[19] C. J. Chang-Hasnain, Y. Zhou, M. C. Y. Huang, and C. Chase, "High-contrast grating VCSELs," *IEEE J. Sel. Topics Quantum Electron.*, vol. 15, no. 3, pp. 869–878, May/Jun. 2009.
[20] D. Fattal, J. Li, Z. Peng, M. Fiorentino, and R. G. Beausoleil, "Flat dielectric grating reflectors with focusing abilities," *Nature Photon.*, vol. 4, no. 7, pp. 466–470, 2010.
[21] C. J. Chang-Hasnain and W. Yang, "High-contrast gratings for integrated optoelectronics," *Adv. Opt. Photon.*, vol. 4, no. 3, pp. 379–440, 2012.
[22] T. Sun, J. Kim, J. M. Yuk, A. Zettl, F. Wang, and C. Chang-Hasnain, "Surface-normal electro-optic spatial light modulator using graphene integrated on a high-contrast grating resonator," *Opt. Exp.*, vol. 24, no. 23, pp. 26035–26043, 2016.
[23] J. A. Giese, J. W. Yoon, B. R. Wenner, J. W. Allen, M. S. Allen, and R. Magnusson, "Guided-mode resonant coherent light absorbers," *Opt. Lett.*, vol. 39, no. 3, pp. 486–488, 2014.

[24] A. L. Fannin, J. W. Yoon, B. R. Wenner, J. W. Allen, M. S. Allen, and R. Magnusson, "Experimental evidence for coherent perfect absorption in guided-mode resonant silicon films," *IEEE Photon. J.*, vol. 8, no. 3, Jun. 2016, Art. no. 6802307.

[25] L. Cao, J. S. White, J.-S. Park, J. A. Schuller, B. M. Clemens, and M. L. Brongersma, "Engineering light absorption in semiconductor nanowire devices," *Nature Mater.,* vol. 8, no. 8, pp. 643–647, 2009.

[26] L. Cao, J.-S. Park, P. Fan, B. Clemens, and M. L. Brongersma, "Resonant germanium nanoantenna photodetectors," *Nano Lett.,* vol. 10, no. 4, pp. 1229–1233, 2010.

[27] E. D. Palik, Ed. *Handbook of Optical Constants of Solids*, vol. 3. San Diego, CA, USA: Academic, 1998.

[28] P. Wu, Z. Chen, D. Xu, C. Zhang, and R. Jian, "A narrow dual-band monolayer unpatterned graphene-based perfect absorber with critical coupling in the near infrared," *Micromachines*, vol. 11, no. 1, 2020, Art. no 58.

[29] F. Lu, F. G. Sedgwick, V. Karagodsky, C. Chase, and C. J. Chang-Hasnain, "Planar high-numerical-aperture low-loss focusing reflectors and lenses using subwavelength high contrast gratings," *Opt. Exp.*, vol. 18, no. 12, pp. 12606–12614, 2010.

[30] V. Karagodsky, F. G. Sedgwick, and C. J. Chang-Hasnain, "Theoretical analysis of subwavelength high contrast grating reflectors," *Opt. Exp.*, vol. 18, no. 16, pp. 16973–16988, 2010.

[31] U. Keller et al., "Semiconductor saturable absorber mirrors (SESAM's) for femtosecond to nanosecond pulse generation in solid-state lasers," *IEEE J. Sel. Topics Quantum Electron.,* vol. 2, no. 3, pp. 435–453, Sep. 1996.

[32] D. Kopf, G. Zhang, R. Fluck, M. Moser, and U. Keller, "All-in-one dispersion-compensating saturable absorber mirror for compact femtosecond laser sources," *Opt. Lett.,* vol. 21, no. 7, pp. 486–488, 1996.

[33] T. Akatsu et al., "Germanium-on-insulator (GeOI) substrates—A novel engineered substrate for future high performance devices," *Mater. Sci. Semicond. Process.,* vol. 9, no. 4, pp. 444–448, 2006.

[34] J. Kang et al., "Focusing subwavelength grating coupler for mid-infrared suspended membrane germanium waveguides," *Opt. Lett.,* vol. 42, no. 11, pp. 2094–2097, 2017.

[35] M. B. Gonzalez et al., "Defect assessment and leakage control in Ge junctions," *Microelectron. Eng.,* vol. 125, pp. 33–37, 2014.

[36] Z. Li et al., "Broadband GaAsSb nanowire array photodetectors for filter-free multispectral imaging," *Nano Lett.*, vol. 21, no. 17, pp. 7388–7395, 2021.

[37] J. Song et al., "High-efficiency and high-speed germanium photodetector enabled by multiresonant photonic crystal," *Nanophotonics*, vol. 10, no. 3, pp. 1081–1087, 2021.

[38] Y. Zhang et al., "Thin germanium waveguide-array-like absorber based on localized resonance," *IEEE Photon. J.,* vol. 14, no. 4, Aug. 2022, Art. no. 4644605.

[39] J. Cui, T. Li, H. Chen, and W. Cui, "High-performance microring resonator Ge-on-Si photodetectors by optimizing absorption layer length," *IEEE Photon. J.*, vol. 12, no. 4, Aug. 2020, Art. no. 6802208.